

Alignment Frustration-Induced Swarming Lattice in the Vicsek-Kuramoto Model

Yichen Lu^{1,2,†}, Yingshan Guo^{1,4,†}, Yiyi Zhang^{1,3}, Tong Zhu^{1,3}, and Zhigang Zheng^{1,3,*}

¹*Institute of Systems Science, Huaqiao University, Xiamen 361021, China*

²*School of Mathematical Sciences, Huaqiao University, Quanzhou, 362021, China*

³*College of Information Science and Technology, Huaqiao University, Xiamen 361021, China*

⁴*College of Mechanical Engineering and Automation Science and Technology, Huaqiao University, Xiamen 361021, China*

(Dated: November 13, 2025)

We introduce a frustration parameter α into the Vicsek-Kuramoto model of self-propelled particles. While the system exhibits conventional synchronized states, such as global phase synchronization and swarming, for low frustration ($\alpha < \pi/2$), beyond the critical point $\alpha = \pi/2$, a Hopf-Turing bifurcation drives a transition to a resting hexagonal lattice, accompanied by spatiotemporal patterns such as vortex lattices and dual-cluster lattices with oscillatory unit-cell motions. Lattice dominance is governed by coupling strength and interaction radius, with a clear parametric boundary balancing pattern periodicity and particle dynamics. Our results demonstrate that purely orientational interactions are sufficient to form symmetric lattices, challenging the necessity of spatial forces and illuminating the mechanisms driving lattice formation in active matter systems.

PACS numbers: 05.45.-a, 89.75.Kd, 05.65.+b

Keywords: active matter, lattice structure, pattern formation, self-organization

The collective motion of self-propelled particles is a fascinating phenomenon observed in various natural and artificial systems, ranging from biological entities like bird flocks [1–3] and fish schools [4, 5] to synthetic active matter such as Janus particles [6–9]. These systems exhibit a wide range of collective behaviors, including clustering [10–13], lane formation [14–16], swirling formations [17–20], cavity formation [21, 22], low-Reynolds-number turbulence [23–25], negative viscosities [26], and even the emergence of crystallization and lattice structures [21, 27–36]. Many of these phenomena have been successfully described by Vicsek-type models, which capture the behavior of particles moving at constant speed and aligning their directions with those of their neighbors under the influence of noise [1]. However, most such formulations rely on spatial interactions—such as repulsion and attraction [21, 35, 36] or stress-induced fluidization [34]—typically associated with high-density systems or strong steric effects. In contrast, purely orientational interactions rarely give rise to symmetric spatial structures independently. This raises a fundamental question: can lattice structures emerge in active matter systems where collective scales far exceed individual scales (e.g., bird flocks) or in low-density, dilute regimes (e.g., gas molecules)?

Since the 2010s, it has been recognized that the Vicsek model can be viewed as a non-equilibrium exten-

sion of the Kuramoto model [37–39], which describes synchronization in networks of coupled phase oscillators, by equating the direction of motion with the oscillator phase [40, 41]. This connection provides a foundational framework for exploring the interplay between self-propulsion and phase coupling, namely the Vicsek-Kuramoto model. Recently, several models integrating self-propulsion and phase interactions have been proposed to study the rich dynamics of orientationally coupled active matter, revealing phenomena such as chirality [20, 42–44], chimeras [45, 46], nematic [43] and anti-aligning interactions [33], non-reciprocal couplings [47], and chemotactic responses [48, 49]. These systems often exhibit macroscopic phase separation and density inhomogeneities. Notably, a model of anti-aligning interactions [33] has demonstrated that particles can self-organize into a traveling hexagonal lattice. This finding implies that phase interactions alone—in the absence of explicit spatial interactions—can give rise to lattice formation. However, the resulting structure is traveling; whether resting lattice patterns can emerge from purely phase-coupling mechanisms remains an open question. Achieving such a static configuration appears challenging for self-propelled particles in the absence of spatial interactions.

In this work, we investigate a minimal model of self-propelled particles with frustrated local alignment, inspired by the Kuramoto-Sakaguchi model for frustrated oscillators [50]. By introducing a frustration parameter, we uncover a rich array of collective states, including synchronization, swarming, vortices, dual clusters, and dual-

[†]These authors contributed equally to this work.

*Corresponding author. zgzheng@hqu.edu.cn

lane patterns. Remarkably, beyond a critical frustration threshold, the system transitions into a resting hexagonal lattice state and exhibits dominance for certain parameter ranges. We systematically map the phase diagram as a function of frustration, coupling strength, and interaction radius. Our analytical results illuminate the mechanisms driving lattice formation in active matter systems.

The Model. Particles are described by position $\mathbf{r}_i = (x_i, y_i)$ and phase angle θ_i , evolving as:

$$\dot{\mathbf{r}}_i = v\mathbf{p}(\theta_i), \quad (1a)$$

$$\dot{\theta}_i = \frac{K}{|A_i|} \sum_{j \in A_i} [\sin(\theta_j - \theta_i + \alpha) - \sin \alpha], \quad (1b)$$

where $A_i(t) = \{j : |\mathbf{r}_i(t) - \mathbf{r}_j(t)| \leq d_0\}$ is the set of neighbors within coupling radius d_0 , $K (\geq 0)$ is coupling strength, and α is frustration. The term $-\sin \alpha$ ensures synchronization ($\theta_j = \theta_i$) remains an equilibrium [51]. This model generalizes alignments [42, 43, 52–54], anti-alignments [33, 55], and chimera states [45, 46]. It reduces to normal Vicsek–Kuramoto for $\alpha = 0$ and anti-aligning interactions for $\alpha = \pi$.

To quantify coordination, we define the single-particle distribution $\rho(\mathbf{r}, \theta, t)$, normalized as $\int_{L^2} d^2\mathbf{r} \int_0^{2\pi} \rho d\theta = 1$, and derive marginalized densities:

$$\varrho(\mathbf{r}, t) = \int_0^{2\pi} \rho(\mathbf{r}, \theta, t) d\theta, \quad (2a)$$

$$p(\theta, t) = \int_{L \times L} \rho(\mathbf{r}, \theta, t) d\mathbf{r}, \quad (2b)$$

where L is system size. The homogeneous solution is $(\rho, \varrho, p) = (\rho_0, \varrho_0, p_0) = (1/(2\pi L^2), 1/L^2, 1/(2\pi))$. Standardized order parameters measure deviations:

$$\rho_{\text{std}}(t) = \frac{1}{1 - \rho_0} \left[\max_{\mathbf{r}, \theta} \rho(\mathbf{r}, \theta, t) - \rho_0 \right], \quad (3)$$

with analogous ϱ_{std} and p_{std} for spatial condensation and phase polarization, respectively. These range in $[0, 1]$, with 0 indicating uniformity and 1 full condensation/polarization.

Lattice Structures and Spatiotemporal Patterns. We now simulate the collective dynamics of N frustrated self-propelled particles in a square domain of size $L \times L$ with periodic boundary conditions; using a time step of $\Delta t = 0.005$. At small α , the system achieves global phase synchronization (Fig. 1(a)), with $p_{\text{std}} = 1$ and $\rho, \varrho_{\text{std}} = 0$, indicating aligned motion and spatial homogeneity. Increasing α leads to a swarming synchronized state (Fig. 1(b)), where particles form a coherent, moving cluster; $p_{\text{std}} = 1$ confirms polarization, while non-zero $\rho_{\text{std}}, \varrho_{\text{std}}$

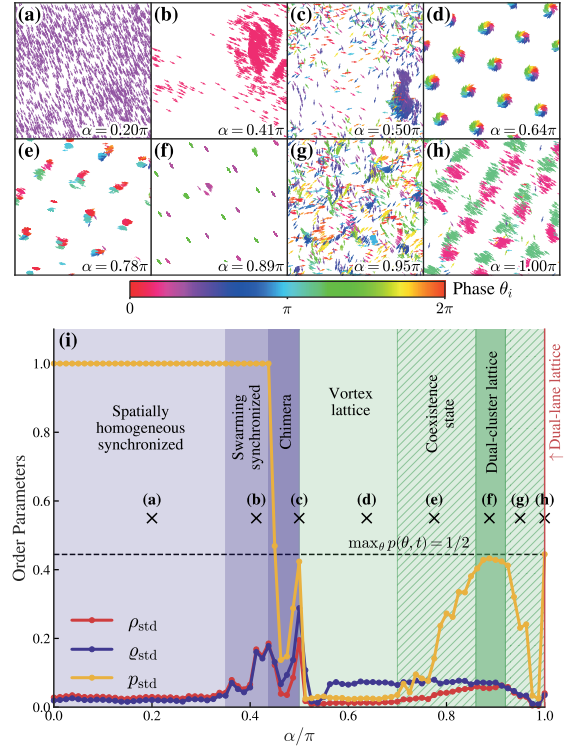


Figure 1. (a)-(h) Spatially homogeneous sync (a), swarming sync (b), chimera (c), vortex lattice (d), dual-cluster lattice (f), dual-lane lattice (h) states, and their coexistence states (e, g), at different frustration α . Arrow orientation/color indicates instantaneous phase θ_i . (i) Phase diagram and order parameters versus α . Blue/green regions (divided by $\alpha = \pi/2$) indicate sync and lattice states, respectively. Dashed horizontal line shows p_{std} when $\max_{\theta} p(\theta, t) = 1/2$ (dual-cluster sync). After reaching a steady state, order parameters were computed by averaging over 500 simulation steps. Other parameters: $K = 20$, $d_0 = 1.55$, $L = 7$, $N = 2000$, $v = 3$.

reflect clustering. For larger $\alpha < \pi/2$, a chimera state emerges (Fig. 1(c)), mixing polarly ordered density cluster and incoherent low-density gas, as the phenomenology studied in [45, 46].

For $\alpha > \pi/2$, lattice states emerge (Fig. 1(d)–(h)). Particles arrange into a hexagonal lattice, with ρ_{std} nearly constant for $0.55\pi < \alpha < 0.9\pi$, indicating stable patterning in spatial density. Meanwhile, p_{std} decreases for $0.5\pi < \alpha < 0.7\pi$, signifying a vortex lattice (Fig. 1(e)), similar to bacterial suspensions [34]. For $0.7\pi < \alpha < \pi$, $p(\theta, t)$ rises, marking a dual-cluster lattice (Fig. 1(f)) with two phase groups differing by π , leading to a bimodal distribution in $p(\theta, t)$ with $\max_{\theta} p(\theta, t) = 1/2$. Approaching $\alpha = \pi$, order parameters decrease, indicating disorder

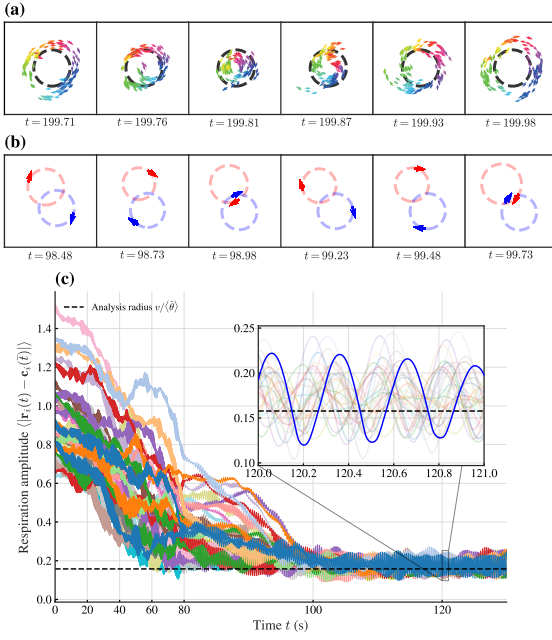


Figure 2. (a, b) Respiration dynamics of vortex (a, $\alpha = 0.6\pi$) and double clustered (b, $\alpha = 0.9\pi$) unit cell. In (b), dashed circle indicates vortex cell volume. In (k), red/blue arrows show phase-divided clusters; dashed circles show estimated trajectories from mean instantaneous frequencies $\langle \dot{\theta}_i \rangle$. (c) Respiration amplitude over time for $\alpha = 0.6\pi$. Other parameters are same as in Fig. 1.

(Fig. 1(g)). At $\alpha = \pi$, anti-synchronization occurs (Fig. 1(h)), forming opposing particle lanes with fixed π phase difference, as seen in the Vicsek model of anti-aligning interaction [56].

Respiration-like Motions. To better understand the spatiotemporal patterns in lattice states, we analyze the dynamics of individual unit cells in the vortex and dual-cluster lattices (Fig. 1(j, k)). In the vortex lattice (Fig. 1(j)), particles undergo a respiration-like motion, periodically expanding and contracting around an average radius of $v/\langle \dot{\theta} \rangle$, where $\langle \dot{\theta} \rangle$, where the mean frequency in incoherent states is

$$\begin{aligned} \langle \dot{\theta} \rangle &= -K \sin \alpha + \frac{K}{2\pi} \int_0^{2\pi} d\theta' \sin(\theta' - \theta + \alpha) \\ &= -K \sin \alpha. \end{aligned} \quad (4)$$

This oscillation is seen in the particle-to-cell-center distance $|\mathbf{r}_i(t) - \mathbf{c}_i(\bar{t})|$, as illustrated in Fig. 1(l), with $\mathbf{c}_i(\bar{t})$ the time-averaged cell center. The dual-cluster lattice (Fig. 1(k)) shows greater order: two condensed particle groups rotate in opposite directions around the unit cell

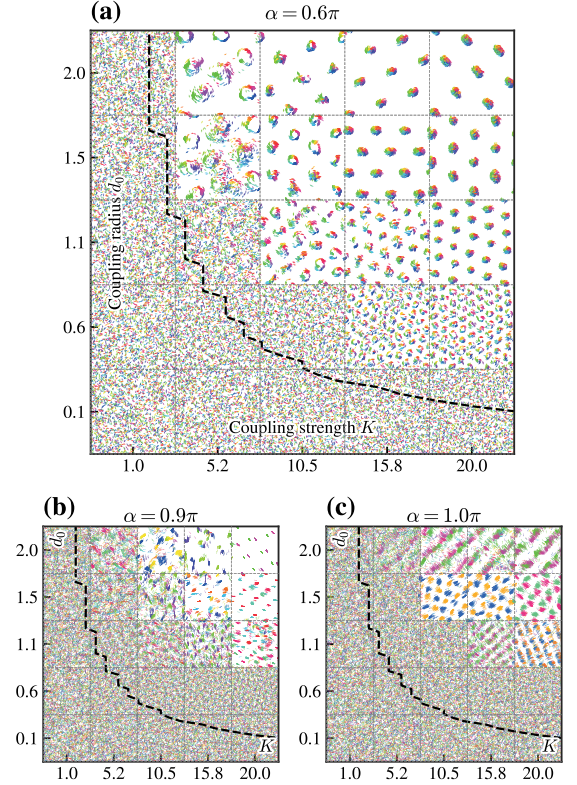


Figure 3. Phase diagrams in the (K, d_0) parameter space for different frustration α ($L = 7, N = 2000, v = 3$). Black dashed lines mark boundaries (Eq. (15)) between dominant and recessive lattice states.

center on near-fixed circular paths (dashed circles), with radii also set by their mean effective frequencies $\langle \dot{\theta}_i \rangle$, as indicated by the dashed circles in Fig. 1(k). These respiration modes arise from a Hopf-Turing bifurcation, as discussed in the section *Critical transition and mechanism*.

Dominant-Recessive Lattice. As discussed above, the lattice state emerges when the frustration α exceeds the critical point $\pi/2$, with α primarily governing the topology of the lattice pattern. However, the prominence of this lattice structure depends on the coupling strength K and coupling radius d_0 . As illustrated in Fig. 3(a)-(c), for a fixed α , a region exists in the high (K, d_0) parameter space where the lattice structure is dominant, characterized by large lattice constants (i.e., the average distance between neighboring unit cells) and large unit cell volumes (i.e., the area occupied by particles within a unit cell). Within this region, the lattice constant increases with d_0 but remains largely unaffected by K . Conversely,

the unit cell volume decreases as K increases but shows minimal dependence on d_0 . Outside this region, the lattice structure becomes recessive, and the system tends toward a more uniform state. The boundary separating these two regimes can be approximated by (15), which reflects a balance between the spatial periodicity of pattern formation and the spatial dynamics of the particles. The sawtooth shape of this boundary stems from the discrete nature of the wavenumber $k_n = 2\pi n/L$ in a finite system with periodic boundary conditions.

Critical transition and mechanism. In the thermodynamic limit $N \rightarrow \infty$, the state of the system in Eq. (1) can be characterized by the single-partial distribution $\rho(\mathbf{r}, \theta, t)$, which satisfies the continuity equation

$$\frac{\partial \rho}{\partial t} = -v\mathbf{p}(\theta) \cdot \nabla \rho - \frac{\partial}{\partial \theta} \{ \mathcal{T}[\rho] \rho \}, \quad (5)$$

where \mathcal{T} is the linear operator that has the form

$$\mathcal{T}[\rho] = \frac{K}{A} \int_{L \times L} d^2 \mathbf{r}' \int_0^{2\pi} d\theta' \rho(\mathbf{r}', \theta', t) \times \Theta(d_0 - |\mathbf{r}' - \mathbf{r}|) [\sin(\theta' - \theta + \alpha) - \sin \alpha], \quad (6)$$

where $\Theta(r)$ is Heaviside step function and

$$A = \int_{L \times L} d^2 \mathbf{r}' \int_0^{2\pi} d\theta' \rho(\mathbf{r}', \theta', t) \Theta(d_0 - |\mathbf{r}' - \mathbf{r}|). \quad (7)$$

One obvious solution of Eq. (5) is $\rho = (2\pi L^2)^{-1}$ representing a uniform disordered state. Inspired by the approaches in [33], the stability of such a solution can be investigated by considering a small perturbation,

$$\rho(\mathbf{r}, \theta, t) = \frac{1}{2\pi L^2} + \varepsilon e^{\lambda(k)t + i\mathbf{k} \cdot \mathbf{r}} \Phi(\theta), \quad (8)$$

with $k = |\mathbf{k}| > 0$, and linearizing the non-linear continuity equation (5), obtaining eigenvalues problem to compute the $\lambda(k)$ spectrum

$$(\mathcal{L}_0 - ivk\mathcal{L}_1) \Phi = \lambda \Phi, \quad (9)$$

\mathcal{L}_0 is diagonal in the basis $\{e^{im\theta}\}_{m=-\infty}^{\infty}$,

$$\mathcal{L}_0 \Phi_m = \lambda_m^{[0]} e^{im\theta}, \quad (10)$$

with the eigenvalues

$$\lambda_m^{[0]}(k) = \frac{K J_1(kd_0)}{kd_0} (\delta_{m,-1} e^{i\alpha} + \delta_{m,1} e^{-i\alpha}), \quad (11)$$

where $J_1(x)$ is the Bessel function of the first kind of order one. The operator \mathcal{L}_1 is defined as

$$\mathcal{L}_1 e^{im\theta} = \frac{1}{2} \left(e^{i(m+1)\theta - i\vartheta} + e^{i(m-1)\theta + i\vartheta} \right), \quad (12)$$

where ϑ is the forms \mathbf{k} with the x axis. Without the loss of generality, we can define the x axis parallel to \mathbf{k} , and, therefore, take $\vartheta = 0$.

For analytical convenience, truncating the expansion at order $M = 2$ gives a 5th-degree characteristic polynomial $P_5(\lambda)$ with the following coefficients:

$$\begin{aligned} c_5 = 1, \quad c_4 = -\frac{2K J_1(d_0 k) \cos \alpha}{d_0 k}, \quad c_3 = \frac{K^2 J_1^2(d_0 k)}{d_0^2 k^2} + k^2 v^2, \\ c_2 = -\frac{K k v^2 J_1(d_0 k) \cos \alpha}{d_0}, \quad c_1 = \frac{3k^4 v^4}{16}, \quad c_0 = 0. \end{aligned} \quad (13)$$

Since $\lambda = 0$ is always a root, we analyze stability using the Routh–Hurwitz criterion on the reduced quartic polynomial $P_4(\lambda)$, yielding the necessary and sufficient condition:

$$J_1(d_0 k) \cos \alpha < 0. \quad (14)$$

This shows stability depends only on α and d_0 , not on K and v . Considering the range of k , d_0 only affect the unstable wave number without altering the qualitative results. And obviously, $\alpha = \pi/2$ is a critical value.

As computations of $\lambda(k)$ shown in Fig. 4(a), for $\alpha < \pi/2$, instability occurs at $k=0$ (type III, no pattern formation, [57]). For $\alpha > \pi/2$, analysis of $P_4(\lambda)$ reveals a Π_0 instability (Hopf-Turing bifurcation), from complex roots with positive real parts, generating spatiotemporal patterns—here, lattice respiration motions. Thus, $\alpha = \pi/2$ is the critical point for lattice emergence.

Most notably, the most unstable wave number $k^*(d_0)$ is largely independent of $\alpha (> \pi/2)$, implying patterns near threshold have similar spatial periodicity. This matches the nearly constant p_{std} unchanged over the interval $\alpha \in (0.55\pi, 0.9\pi)$ in Fig. 1(i) and the observed constant lattice spacing in simulations (Fig. 4(c)), predictable via wavelength $2\pi/k_n^*(d_0)$.

Significantly, apart from spatial periodicity, the volume of the unit cell is another important characteristic of the lattice state. For the vortex lattice near $\alpha = \pi/2$, phase is incoherent, and the mean effective rotational radius is approximately $v/|\dot{\theta}_i| \approx v/K$. The lattice emergence condition balances pattern periodicity and particle dynamics, occurring when two unit cells tangent, i.e., cell diameter equals wavelength:

$$\frac{2\pi}{k^*(d_0)} = \frac{2v}{K}, \quad (15)$$

This matches the (K, d_0) phase diagram (Fig. 3(a)-(c)). When the wavelength is too short to accommodate the unit cell volume, the cells overlap, leading to macroscopic uniformity.

Conclusions. Frustrated alignment in the Vicsek-Kuramoto model can induce a resting hexagonal lattice

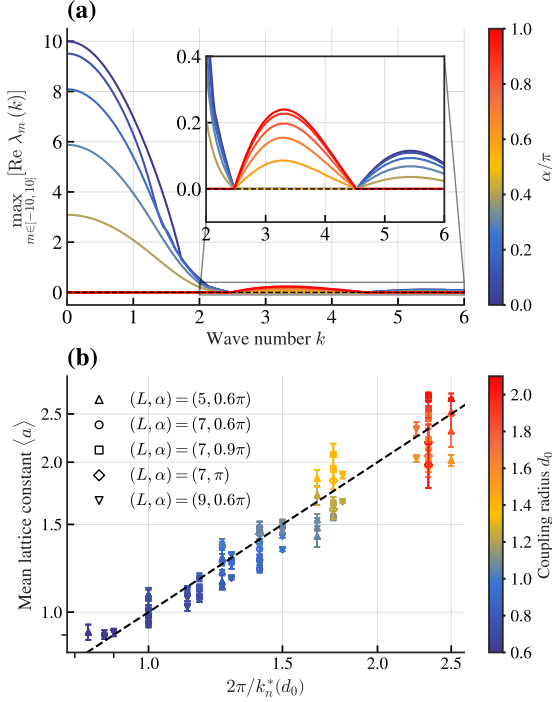


Figure 4. (a) Computations of the $\lambda(k)$ with the largest real part as a function of the continuous wavenumber k and α in the truncated basis $M = 10$. Other parameters as in Fig. 1. (b) Measured mean lattice constant $\langle a \rangle$ compared to theoretical prediction. Horizontal and vertical error bars represent standard deviations across K and unit cells, respectively. The black dashed line indicates a 1:1 correspondence.

structure in self-propelled particles, demonstrating that purely orientational interactions are sufficient for symmetric pattern formation without explicit spatial forces. This system exhibits a rich array of collective states: For low frustration parameters ($\alpha < \pi/2$), it achieves synchronized states such as global synchronization and swarming, whereas beyond the critical point ($\alpha > \pi/2$), it transitions into lattice patterns including vortex lattices and dual-cluster lattices, as visualized in the spatial configurations (Fig. 1). The critical transition at $\alpha = \pi/2$ is characterized by a Hopf-Turing bifurcation, leading to spatiotemporal patterns with respiration-like dynamics within the unit cells (Fig. 2). The dominance of the lattice structure depends on the coupling strength and radius, with a clear boundary in the (K, d_0) parameter space (Fig. 3), explained by balancing pattern periodicity and particle dynamics (Eq. (15)). This work establishes frustration as a design principle for tuning lattice topology in active matter systems, but leaves open questions regarding the stability of pattern selection and the prediction of respiration frequencies, warranting further investigation to characterize the nature of these emergent structures.

Acknowledgments. We are grateful to Professor Yunyun Li at Tongji University for fruitful discussions. This work is partially supported by National Natural Science Foundation of China (Nos. 12375031 and 11875135).

-
- [1] T. Vicsek, A. Czirók, E. Ben-Jacob, I. Cohen, and O. Shochet, *Phys. Rev. Lett.* **75**, 1226 (1995).
- [2] W. Bialek, A. Cavagna, I. Giardina, T. Mora, E. Silvestri, M. Viale, and A. M. Walczak, *Proceedings of the National Academy of Sciences* **109**, 4786 (2012).
- [3] H. Qiu, C. Wei, R. Dou, and Z. Zhou, *Science China Information Sciences* **58**, 1 (2015).
- [4] M. Ballerini, N. Cabibbo, R. Candelier, A. Cavagna, E. Cisbani, I. Giardina, V. Lecomte, A. Orlandi, G. Parisi, A. Procaccini, M. Viale, and V. Zdravkovic, *Proceedings of the National Academy of Sciences* **105**, 1232 (2008).
- [5] A. D. Becker, H. Masoud, J. W. Newbolt, M. Shelley, and L. Ristroph, *Nature Communications* **6**, 8514 (2015).
- [6] A. Walther and A. H. E. Müller, *Soft Matter* **4**, 663 (2008).
- [7] A. Walther and A. H. E. Müller, *Chemical Reviews* **113**, 5194 (2013), pMID: 23557169.
- [8] A. I. Campbell, S. J. Ebbens, P. Illien, and R. Golestanian, *Nature Communications* **10**, 3952 (2019).
- [9] S. J. Ebbens and D. A. Gregory, *Accounts of Chemical Research* **51**, 1931 (2018), pMID: 30070110.
- [10] Y. Zhou, Y. Li, and F. Marchesoni, *Chinese Physics Letters* **40**, 100505 (2023).
- [11] I. Buttinoni, J. Bialké, F. Kümmel, H. Löwen, C. Bechinger, and T. Speck, *Phys. Rev. Lett.* **110**, 238301 (2013).
- [12] K. Ishimoto and E. A. Gaffney, *Scientific Reports* **8**, 15600 (2018).
- [13] R. M. Navarro and S. M. Fielding, *Soft Matter* **11**, 7525 (2015).
- [14] C. W. Wächter, F. Kogler, and S. H. L. Klapp, *Phys. Rev. E* **94**, 052603 (2016).
- [15] F. Kogler and S. H. L. Klapp, *Europhysics Letters* **110**, 10004 (2015).
- [16] T. Vissers, A. Wysocki, M. Rex, H. Löwen, C. P. Royall, A. Imhof, and A. van Blaaderen, *Soft Matter* **7**, 2352 (2011).
- [17] A. Kudrolli, G. Lumay, D. Volfson, and L. S. Tsimring, *Phys. Rev. Lett.* **100**, 058001 (2008).
- [18] I. H. Riedel, K. Kruse, and J. Howard, *Science* **309**, 300

- (2005).
- [19] C. Dombrowski, L. Cisneros, S. Chatkaew, R. E. Goldstein, and J. O. Kessler, *Phys. Rev. Lett.* **93**, 098103 (2004).
- [20] Y. Lu, Y. Xu, W. Cai, Z. Tian, J. Xu, S. Wang, T. Zhu, Y. Liu, M. Wang, Y. Zhou, C. Yan, C. Li, and Z. Zheng, *Chaos, Solitons & Fractals* **191**, 115794 (2025).
- [21] R.-x. Guo, J.-j. Li, and B.-q. Ai, *Phys. Rev. E* **111**, 045423 (2025).
- [22] Y. Zhou, Q. Yin, S. Nayak, P. Bag, P. K. Ghosh, Y. Li, and F. Marchesoni, *Large-scale dynamics in visual quorum sensing chiral suspensions* (2025), arXiv:2508.11254 [cond-mat.soft].
- [23] G. Kokot, S. Das, R. G. Winkler, G. Gompper, I. S. Aranson, and A. Snezhko, *Proceedings of the National Academy of Sciences* **114**, 12870 (2017).
- [24] H. Reinken, S. H. L. Klapp, M. Bär, and S. Heidenreich, *Phys. Rev. E* **97**, 022613 (2018).
- [25] C. Reichhardt, J. Thibault, S. Papanikolaou, and C. J. O. Reichhardt, *Phys. Rev. E* **98**, 022603 (2018).
- [26] D. Saintillan, *Annual Review of Fluid Mechanics* **50**, 563 (2018).
- [27] N. Kumar, R. Zhang, J. J. de Pablo, and M. L. Gardel, *Science Advances* **4**, eaat7779 (2018).
- [28] S. Praetorius, A. Voigt, R. Wittkowski, and H. Löwen, *Phys. Rev. E* **97**, 052615 (2018).
- [29] I. Theurkauff, C. Cottin-Bizonne, J. Palacci, C. Ybert, and L. Bocquet, *Phys. Rev. Lett.* **108**, 268303 (2012).
- [30] R. Thar and M. Kühl, *Applied and Environmental Microbiology* **68**, 6310 (2002).
- [31] R. Thar and M. Kühl, *FEMS Microbiology Letters* **246**, 75 (2005).
- [32] J. Palacci, S. Sacanna, A. P. Steinberg, D. J. Pine, and P. M. Chaikin, *Science* **339**, 936 (2013).
- [33] D. Escaff, *Phys. Rev. E* **109**, 024602 (2024).
- [34] H. Xu and Y. Wu, *Nature* **627**, 553 (2024).
- [35] R. Olfati-Saber, *IEEE Transactions on Automatic Control* **51**, 401 (2006).
- [36] G. Wang, M. Liu, F. Wang, and Y. Chen, *IEEE Control Systems Letters* **7**, 1159 (2023).
- [37] J. A. Acebrón, L. L. Bonilla, C. J. Pérez Vicente, F. Ritort, and R. Spigler, *Rev. Mod. Phys.* **77**, 137 (2005).
- [38] F. A. Rodrigues, T. K. D. Peron, P. Ji, and J. Kurths, *Physics Reports* **610**, 1 (2016).
- [39] Z. Zheng, *Emergence Dynamics in Complex Systems: From Synchronization to Collective Transport* (Science Press, Beijing, 2019).
- [40] F. D. C. Farrell, M. C. Marchetti, D. Marenduzzo, and J. Tailleur, *Phys. Rev. Lett.* **108**, 248101 (2012).
- [41] P. DEGOND, G. DIMARCO, and T. B. N. MAC, *Mathematical Models and Methods in Applied Sciences* **24**, 277 (2014).
- [42] B. Liebchen and D. Levis, *Phys. Rev. Lett.* **119**, 058002 (2017).
- [43] B. Ventejou, H. Chaté, R. Montagne, and X.-q. Shi, *Phys. Rev. Lett.* **127**, 238001 (2021).
- [44] Y.-C. Lu, W.-R. Cai, M.-C. Wang, Y.-L. Liu, T. Zhu, Y.-L. Zhou, T.-C. Yu, Y.-X. Ji, M.-Q. Ao, C.-L. Li, C.-X. Yan, and Z.-G. Zheng, *Chinese Physics B* **34**, 080506 (2025).
- [45] N. Kruk, Y. Maistrenko, and H. Koepl, *Phys. Rev. E* **98**, 032219 (2018).
- [46] N. Kruk, J. A. Carrillo, and H. Koepl, *Phys. Rev. E* **102**, 022604 (2020).
- [47] K. L. Kreienkamp and S. H. L. Klapp, *New Journal of Physics* **24**, 123009 (2022).
- [48] B. Liebchen, M. E. Cates, and D. Marenduzzo, *Soft Matter* **12**, 7259 (2016).
- [49] A. Ziepkke, I. Maryshev, I. S. Aranson, and E. Frey, *Nature Communications* **13**, 6727 (2022).
- [50] H. Sakaguchi and Y. Kuramoto, *Progress of Theoretical Physics* **76**, 576 (1986).
- [51] H. Sakaguchi, S. Shinomoto, and Y. Kuramoto, *Progress of Theoretical Physics* **79**, 1069 (1988).
- [52] D. Levis, I. Pagonabarraga, and B. Liebchen, *Phys. Rev. Res.* **1**, 023026 (2019).
- [53] D. Escaff and R. Delpiano, *Chaos: An Interdisciplinary Journal of Nonlinear Science* **30**, 083137 (2020).
- [54] Y. Wang, B. Ventéjou, H. Chaté, and X.-q. Shi, *Phys. Rev. Lett.* **133**, 258302 (2024).
- [55] D. Escaff, *Phys. Rev. E* **110**, 024603 (2024).
- [56] P. Bisht, *Lanes and lattice structures in a repulsive model for self-propelled agents* (2024), arXiv:2412.10577 [cond-mat.soft].
- [57] M. C. Cross and P. C. Hohenberg, *Rev. Mod. Phys.* **65**, 851 (1993).